Polymer 50 (2009) 2304–2319

Contents lists available at ScienceDirect

Polymer

journal homepage: www.elsevier.com/locate/polymer

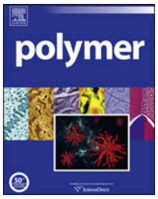

Structure–property relations in molded, nucleated isotactic polypropylene

Jan-Willem Housmans [a,b], Markus Gahleitner [c], Gerrit W.M. Peters [a,*], Han E.H. Meijer [a]

[a] Department of Mechanical Engineering, Eindhoven University of Technology, P.O. Box 513, 5600MB Eindhoven, The Netherlands
[b] The Dutch Polymer Institute (DPI), P.O. Box 902, 5600 AX Eindhoven, The Netherlands
[c] Borealis GmbH, Innovation Center Linz, A-4021 Linz, Austria

ARTICLE INFO

Article history:
Received 30 September 2008
Received in revised form
26 February 2009
Accepted 27 February 2009
Available online 27 March 2009

Keywords:
Polypropylene
Nucleating agent
Processing structure–property relation

ABSTRACT

The influence of molecular characteristics and nucleating agents on the morphology distribution and properties of injection molded isotactic polypropylene (iPP) is investigated using optical microscopy, X-ray diffraction and mechanical testing. To have better control over the thermo-mechanical history, instead of a reciprocating screw, a capillary rheometer is used to drive the melt into the simple rectangular mold. Molecular weight (MW), molecular weight distribution (MWD) and addition of ethylene via copolymerization all influence the thickness of the oriented shear layer, the crystallinity, the type and amount of crystal phases, and the lamellar thickness. The addition of a nucleating agent (DMDBS), dictates the crystallization process, and resulting morphology, and samples with an oriented morphology over the full thickness are created without changing other morphological features, by applying a thermal treatment to the melt prior to injection, which is based on the specific phase behavior of the iPP-DMDBS system. The thermally treated samples show a considerable improvement in mechanical properties.

1. Introduction

The market share of polypropylene increases steadily due to a favorable combination of price and performance, and the possibility to modify the polymer to broaden its range of properties [1]. Long chains, for example, greatly enhance the formation of threadlike structures [2–6], illustrating that molecular details and processing conditions applied determine morphology and thus properties of the product. The effect of processing conditions on the crystallization kinetics and structure development of semi-crystalline polymers has been studied extensively [4–12]. Flow accelerates crystallization and alters morphology, and the effect of shear rate is more pronounced than that of the shear time.

Material modifications are implemented on the molecular or the microscopic level. In the first case, the polymer chain itself is changed, e.g. via long chain branching or copolymerization, while in the second case, e.g. particles, or a phase separated second polymer, are added. These modifications change the crystallization kinetics of the polymer, the final morphology and thus the resulting properties, see e.g. [13–21].

Most of the crystallization studies mentioned apply a short-term shearing protocol as originally introduced by Janeschitz-Kriegl and co-workers [8], or some variations thereof, to separate the effect of flow and temperature on the crystallization behavior. The conditions applied are, however, far from those occurring in injection molding, which is one of the most common industrial production processes to shape plastic parts. In injection molding the polymer is fed via a hopper into a screw extruder where it is molten, using as sources external heaters and the heat dissipation in the flow. Via the reciprocating screw moving forward the melt is pushed via the runners into the product cavity, and made to solidify adopting the shape of the cavity, whereafter the mold is opened to eject the product. With this production process, complex-shaped products can be realized with molds consisting of multiple parts and slides, including rotational molds that allow for multi-shot processing using 2 injection units. The thermo-mechanical history experienced by the polymer is complex due to the high deformation rates, the high pressures (compressibility of the polymer) and speeds applied, the geometry of the feeding system and the mold that induces complex flow fields and the high temperature gradients and high cooling rates. Complex histories starting in the screw are sometimes reflected in the complex morphologies found in the product [22]. In this example [22], the authors used a nylon 6 nanocomposite, and observed in cross-sections of their samples, perpendicular to flow direction, dark–light layer sequences in birefringence that were traced back all the way to the sprue section and the explanation given was that these layers are formed already during the melting and conveying in the screw, and subsequently are transported downstream.

---

[*] Corresponding author. Tel.: +31 40 247 4840; fax: +31 40 244 7355.
E-mail address: g.w.m.peters@tue.nl (G.W.M. Peters).

0032-3861/$ – see front matter © 2009 Elsevier Ltd. All rights reserved.
doi:10.1016/j.polymer.2009.02.050

Examples like these illustrate the complexity of the analysis of relations between morphology and processing conditions, and their effects on properties, since the full thermo-mechanical history, starting from the point where the polymer enters the screw extruder, sometimes has to be taken into account. In the first patented injection molding machine, used to produce celluloid billiard balls, a plunger forced the material from a cylindrical reservoir into the mold [23]. Compared to machines equipped with screws, the advantage is that by melting the material in a reservoir, it enables to remove the thermo-mechanical history of prior manufacturing. Disadvantages, of course, are the loss of continuity in the production process, and the reduced homogeneity in the absence of the screw's mixing capacity. A capillary rheometer has a configuration similar to that of the patent, and is designed to determine rheological properties via forcing a melt with a well-defined initial thermo-mechanical state through a capillary or slit geometry. The rheometer can also act as an injection molding machine when the capillary is exchanged with a mold to produce test samples. Since we do not care about production continuity, a capillary rheometer is used as a model injection molding machine.

The primary objective of this work is to study the effect of molecular structure, thus molecular weight (MW), molecular weight distribution (MWD) and the amount of ethylene comonomer, and nucleating agents on the final morphology of molded samples. The morphology distribution is determined from optical microscopy (OM), revealing different structural layers, and X-ray diffraction from which crystallinity, crystal type and lamellar thickness are determined. A thermal treatment is given to the nucleated samples prior to injecting to make use of the thermo-reversibility of the blend to finally create samples with an oriented morphology over its complete thickness. Mechanical tests reveal that, due to this thermal treatment, both the modulus and strain at break increase compared to the untreated samples. Pure iPP shows the same improvement in properties, when given the same thermal treatment as the nucleated samples.

Table 1
Molecular and physical properties of the materials used.

Material	Code	M_w [kg mol^{-1}]	M_w/M_n [−]	E-content [mol%]	DMDBS [wt%]	T_m [°C]	T_c [°C]
HD234CF	PP1	310	3.4	0	0	159	110
HD120MO	PP2	365	5.4	0	0	163	113
13E10	PP3	636	6.9	0	0	163	117
RD204CF	RACO1	310	3.4	3.4	0	147	105
RD226CF	RACO2	310	3.4	5.4	0	140	99
RD208CF	RACO3	310	3.4	7.3	0	138	98
PP2 + DMDBS	PP2_03	365	5.4	0	0.3	165	131
PP2 + DMDBS	PP2_07	365	5.4	0	0.7	165	132
PP2 + DMDBS	PP2_10	365	5.4	0	1.0	165	132

The detailed analysis of such experiments, with transient non-Newtonian, non-isothermal flow and simultaneously solidifying layers, is part of a parallel project [24,25]. Such analysis is only possible when rheological, thermal, specific volume, quiescent crystallization and flow induced crystallization data are available, together with a full numerical model incorporating all conservation laws. Moreover, to compare the presented experimental results with the outcomes of numerical simulations it is of utmost importance to know the initial state of the material and all boundary conditions (thermal and mechanical), one of the main reasons to consciously design these experiments such that these are known. Only then the experimental results can be used for such analysis and, in this way, for validation of the models used. After taking this long but essential route, application to more complex molding systems is allowed.

2. Experimental

2.1. Materials

Materials used are three isotactic polypropylene grades (iPP) Borealis HD234CF, Borealis HD120MO and DSM 13E10, which are coded PP1, PP2 and PP3, respectively, and three propylene/ethylene random copolymer grades (P/E RaCo) Borealis RD204CF, RD226CF

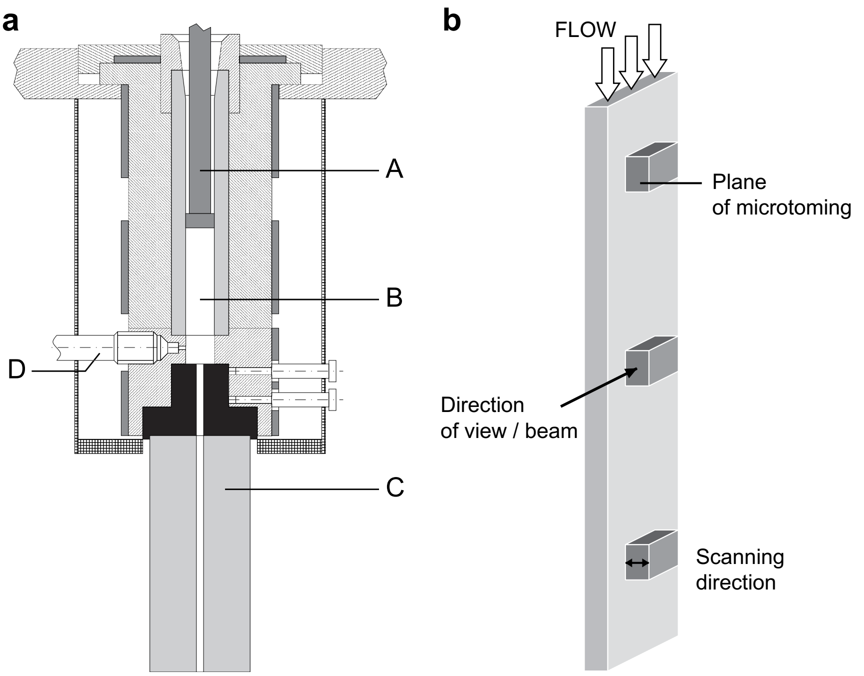

Fig. 1. (a) Capillary rheometer. A = Piston, B = Material reservoir, C = Rectangular shaped mold, D = Pressure transducer. (b) Illustration of a rectangular sample, indicating flow direction, plane of microtoming, direction of view (LM), beam and scanning (X-ray).

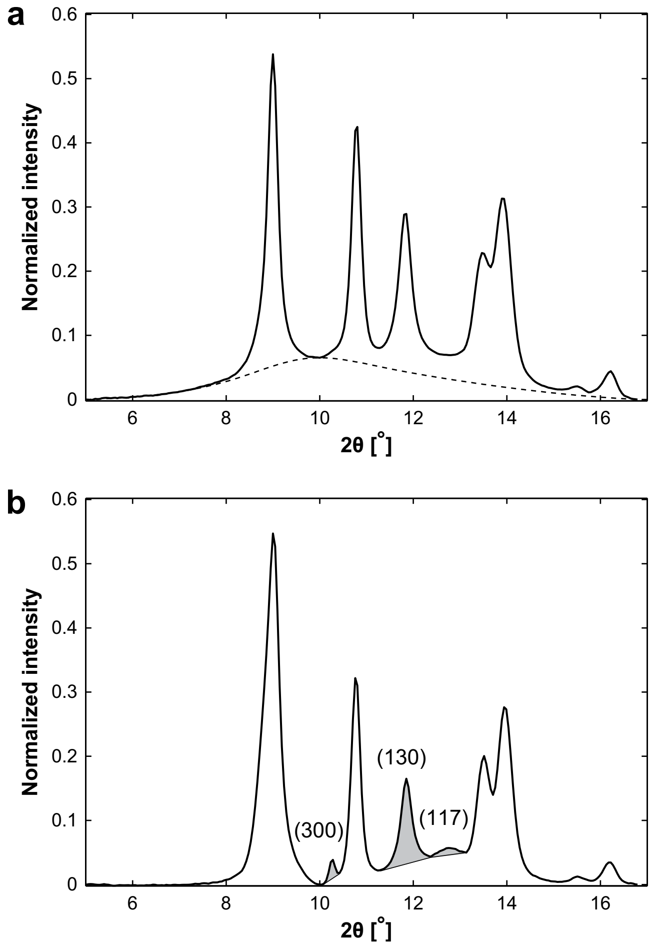

Fig. 2. (a) Normalized intensity versus 2θ for a PP2 sample measured in the core. The dashed line is the underlying amorphous halo. (b) WAXD pattern after subtraction of the amorphous halo. The shaded areas indicate the reflections of the α (130), β (300) and γ (117) phase, which are used for the quantification of the different phases.

and RD208CF with different ethylene contents which are labeled RACO1, RACO2 and RACO3, respectively. A nucleating agent, 1,3:2,4-bis(3,4-dimethylbenzylidene)-sorbitol (DMDBS, Millad 3988, Milliken Chemical, Belgium) is added to PP2 in different concentrations. In relatively small amounts ($\sim$0.2 wt%) DMDBS enhances clarity and gives rise to an increase in yield stress [16,17]. It dissolves at high temperatures into the iPP melt which improves their mixing. During cooling the additive phase separates and self-organizes into microfibrillar structures forming a network in the polymer melt on top of which crystals grow radially [18,26,27]. Molecular and physical properties are listed in Table 1. The materials have been used in several crystallization studies [4,16,18–21,28–37], in which also detailed rheological, thermal and crystallization data of these materials are given.

2.2. Sample preparation

Prior to blending, pellets of PP2 were pulverized in a freezer mill (Retsch ZM100, F. Kurt Retsch GmbH & Co. KG, Germany). Various dry-blended mixtures of iPP and 0.3, 0.7 and 1.0 wt% DMDBS were compounded in a laboratory, corotating mini-twin-screw extruder (DSM Xplore 15 ml microcompounder) in a nitrogen atmosphere for 10 min at a temperature of 240 °C, 250 °C and 260 °C, respectively. The temperatures were determined from the melting temperature/composition diagrams of the system i-PP/DMDBS [16].

Table 2

(hkl) Reflections for the α, β and γ phase and the peak positions for the mesomorphic phase of isotactic polypropylene. The 2θ diffraction angles are given for wavelengths $\lambda = 0.98399$ Å (ESRF, ID13) and $\lambda = 1.54$ Å.

$(hkl)_\alpha$	$(hkl)_\beta$	$(hkl)_\gamma$	meso	d-Value [Å]	2θ ($\lambda = 0.98$ Å)	2θ ($\lambda = 1.54$ Å)
		(111)		6.39	8.83	13.86
(110)				6.26	9.02	14.14
			x	5.98	9.44	14.8
		(113)		5.86	9.63	15.11
	(300)			5.50	10.26	16.10
(040)				5.24	10.78	16.92
		(008)		5.20	10.86	17.02
(130)				4.78	11.82	18.55
		(117)		4.38	12.90	20.27
(111)		(202)		4.17	13.55	21.31
			x	4.07	13.88	21.8
$(13\bar{1})/(041)$		(026)		4.05	13.96	21.86
		(206)		3.63	15.58	24.53
(150)/(060)				3.51	16.12	25.35
		(00 12)		3.47	16.30	25.65
(200)				3.28	17.25	27.18

The solidified strings of material from the extruder were chopped into pellets. The samples are coded 'PP2' plus the concentration, e.g. PP2_07 for the blend with 0.7 wt% DMDBS.

2.3. Capillary rheometer

A capillary rheometer (Rheograph 6000, Göttfert Werkstoff-Prüfmachinen GmbH, Germany) was adjusted to act as model injection molding machine, Fig. 1(a). The rheometer has a cylindrical material reservoir (Ø12*mm*) in which the polymers are molten and a piston which forces the polymer melt into the rectangular shaped mold with an open end (dimensions sample geometry: $2 \times 12 \times 135$ mm, Fig. 1(b)). The mold is cooled thermostatically to approximately 20 °C with a cooling clamp through which water flows continuously.

Samples of the pure iPP grades were prepared by melting the pellets as received in the material reservoir for 10 min at 220 °C, and subsequent injection molding with different piston speeds (5, 10, 20 and 40 mm s^{-1} for 16,8,4 and 2 s respectively.). The homopolymer PP1 and the RaCo grades were processed with the same conditions as the grades PP2 and PP3 except that the lowest injection speed was discarded. The i-PP/DMDBS blends were molten at 230 °C (PP2_03 and PP2_07) and 240 °C (PP2_10) for 10 min, before injection molding with a piston speed of 20 mm s^{-1} for 4 s. The maximum speed of the capillary rheometer is 40 mm s^{-1}, which gives an apparent shear rate at the wall of the cavity of $\dot{\gamma} = 565\ s^{-1}$, which is still relatively low compared to the maximum shear rates that are reached with an injection molding machine O(10,000–100,000) s^{-1}, e.g. [38].

2.4. Optical microscopy

Optical light microscopy (OM) was used to visualize structural layers over the thickness of the sample (view direction = vorticity direction) at three different positions in the center of the sample, Fig. 1(b), to determine the layer thicknesses. Cross-sections of 3–7 μm were prepared at low temperatures of approximately −130 °C using liquid nitrogen at a rotary microtome (Reichert Ultracut E) equipped with a glass knife. Optical micrographs were taken between crossed polarizers, ±45° rotated with respect to the flow direction, with an Axioplan imaging microscope and the combined Axio Cam camera.

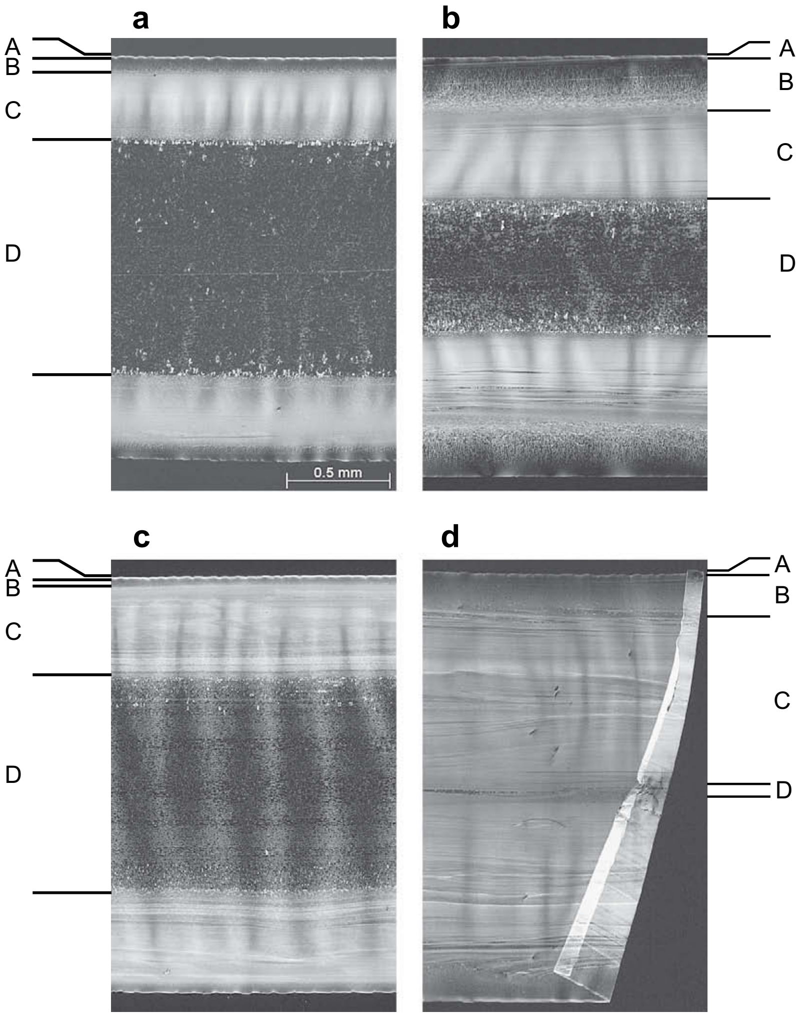

Fig. 3. Optical micrographs of cross-sections of 2 injection molded iPP samples: (a) PP2, 40 mm s^{-1} for 2 s, (b) PP2, 5 mm s^{-1} for 16 s, (c) PP3, 40 mm s^{-1} for 2 s and (d) PP3, 5 mm s^{-1} for 16 s. Distinguished layers are: the 'skin layer' (A), the 'transition layer' (B), the 'shear layer' (C) and the 'isotropic core' (D).

2.5. *X-ray diffraction*

Combined Wide Angle X-ray Diffraction (WAXD) and Small Angle X-ray Scattering (SAXS) experiments were performed at the microfocus beamline ID13 of the European Synchrotron Radiation Facility (ESRF) in Grenoble, France. The size of the X-ray beam is 10 μm having a wavelength of 0.98399 Å. The detector used is a MAR CCD detector with 2048 × 2048 pixels using 2 by 2 rebinning to reduce the size of the data files. Both horizontal and vertical pixel sizes are 157.9 μm. From calibration experiments using silver behenate a sample-to-detector distance of 178.9 mm was determined. Due to beam decay, working with constant exposure time would yield scattering patterns with different scattering intensities which can give problems with background subtraction. At ID13 it is possible to keep the total scattering intensity of each pattern constant, i.e. an increasing exposure time with the decaying beam, such that the background can be subtracted fully (without a scale factor). Data scans are performed over the thickness of central part of the samples with scan steps of 50 μm, see Fig. 1(b).

2.6. *Structural analysis*

The diffraction patterns contain a lot of information on the morphology distribution of the samples. From the combined SAXS/WAXD measurements the crystallinity, the type and amount of crystals and their lamellar thickness, among others, can be obtained. Circular integration of the (corrected) two-dimensional (2D) diffraction patterns gives intensity ($I(2\theta)$) versus diffraction

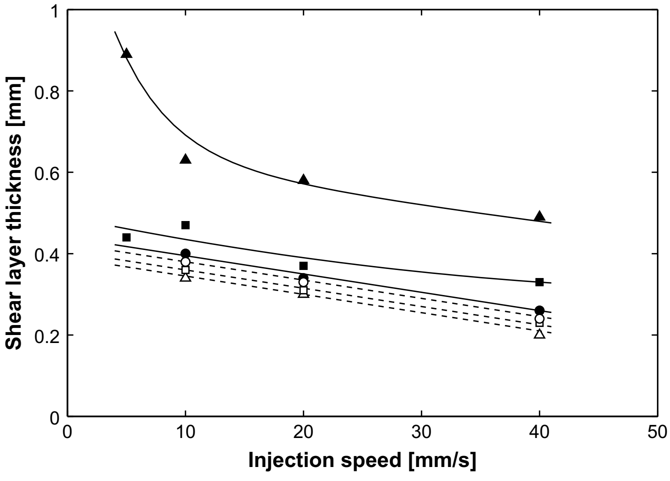

Fig. 4. Shear layer thickness as a function of injection speed for the pure iPP grades, PP1 (●), PP2 (■) and PP3 (▲), and the RaCo's, RACO1 (○), RACO2 (□) and RACO3 (△).

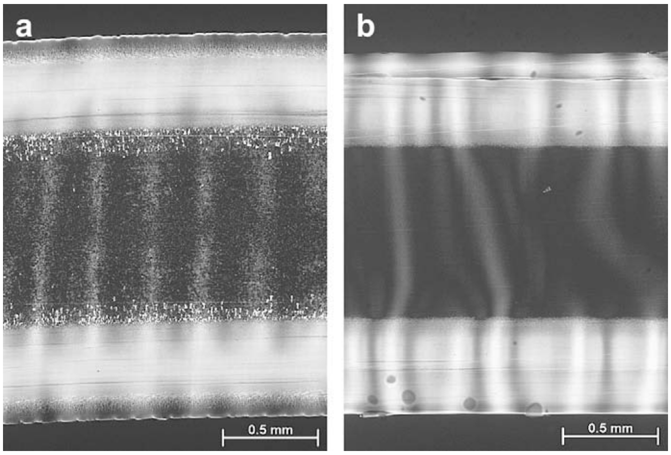

Fig. 5. Optical micrographs of cross-sections of samples injection molded with 20 mm s^{-1} for 4 s: (a) PP2 and (b) PP2_03.

angle, 2θ, consisting of a crystalline and an amorphous part. Crystallinity (X_c) can be quantified according to:

$$X_c = \frac{A_c}{A_{total}} \tag{1}$$

with $A_c = A_{total} - A_a$ the area of the crystalline peaks, A_{total} the area of the total pattern and A_a that of the amorphous halo. The amorphous halo is measured at room temperature, immediately after quenching of a low-isotactic sample (36.7% *mmmm*) having negligible crystallinity [39,40]. The amorphous halo was scaled by equating the maximum of the amorphous halo to the minimum between the $(110)_\alpha$ and the $(040)_\alpha$ diffraction peaks. This is graphically demonstrated in Fig. 2(a).

A common phenomenon observed for iPP is polymorphism, i.e. the polymer can crystallize into different types of crystal phases, the α, β, γ and mesomorphic phase. Under standard conditions the α phase with a monoclinic crystal structure is formed, characterized by so-called cross-hatching or lamellar branching [41,42], consisting of daughter lamellae that grow on top of the initial (mother) lamellae under an angle of ~80° or 100°. The β phase with its hexagonal unit cell is formed when the polymer crystallizes (i) in the presence of a temperature gradient [43], (ii) under conditions like a strong imposed orientation [44–46] and (iii) in the presence of certain nucleating agents [47–49]. Occurrence of the γ phase, with its orthorhombic unit cell, is determined by the molecular structure: (i) low stereo-regularity of the chains [39,40,50], (ii) a low molecular weight [51] and (iii) copolymerization with for instance ethylene [52]. Also in crystallization at elevated pressures γ crystal structures are sometimes observed [39,40,53]. Finally, the mesomorphic crystal phase is only found when the polymer is cooled very rapidly [60,61].

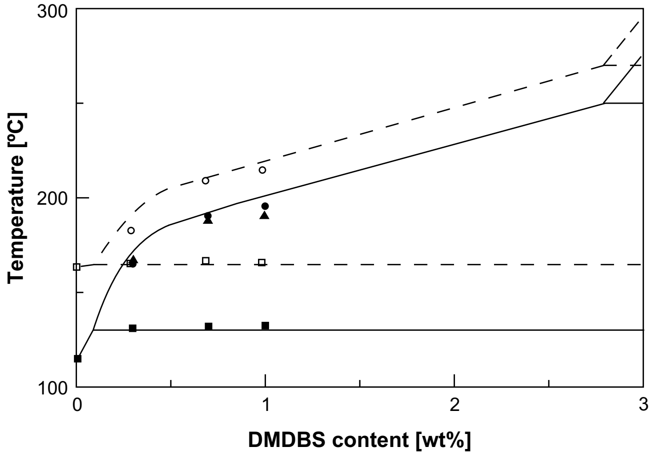

Fig. 6. Phase diagrams for PP2-DMDBS, solid line/closed symbols = cooling diagram and dashed line/open symbols = heating diagram. (■, □, ▲) determined with DSC, (●, ○) determined with rheology.

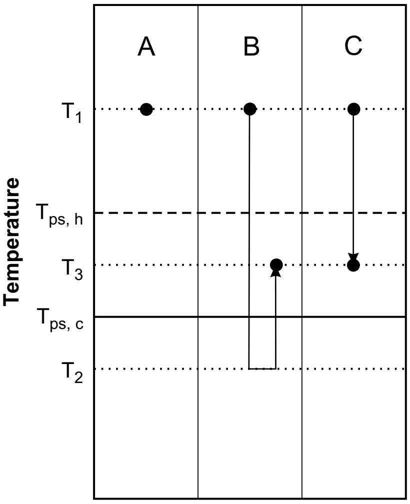

Fig. 7. Graphical representation of the thermal treatment described in the text. For the temperature values for every concentration: see Table 3.

The different types of crystals have their own crystal planes with a specific d-spacing between the planes and thus a specific WAXD pattern, summarized in Table 2 [54–56]. Most of the diffraction peaks of the different crystal phases overlap and have almost the same diffraction angle, but for each phase one peak can be attributed to be specific, identified as the $(130)_\alpha$, the $(300)_\beta$ and the$(117)_\gamma$ peak. These reflections are used to determine the fraction of different crystal types. Several methods are applied, either to determine the fraction of α and β phase [57,58] or of α and γ phase [39,56,59]. This method works as long as the third crystal type, either γ or β, respectively, is not present. Some methods use the area under the peaks [39,58] others the height of the peaks [56,57,59]. We use the first and define the fraction (X_i) of a specific crystal type as:

$$X_i = \frac{A_i}{A_\alpha + A_\beta + A_\gamma} \tag{2}$$

with i the specific crystal phase (either α, β or γ) and A_i the area under the peak of the specific phase. Since the peaks partially overlap, exact determination is a little more difficult, and Fig. 2(b) illustrates the method used, following van der Burgt et al. [39,40].

In general, iPP crystallizes from nuclei into folded chain crystals. In between these lamellae unordered amorphous material is present. These two regions have a different electron density and will therefore scatter an X-ray beam at small angles. The position of the scattering peak is related to the long period (L), which is the distance between two lamellae, i.e. the combination of a crystal lamella plus the amorphous region between two lamellae. From Bragg's law (equation (3)) the long period can be calculated with equation (4).

$$n\lambda = 2d\ \sin\theta \tag{3}$$

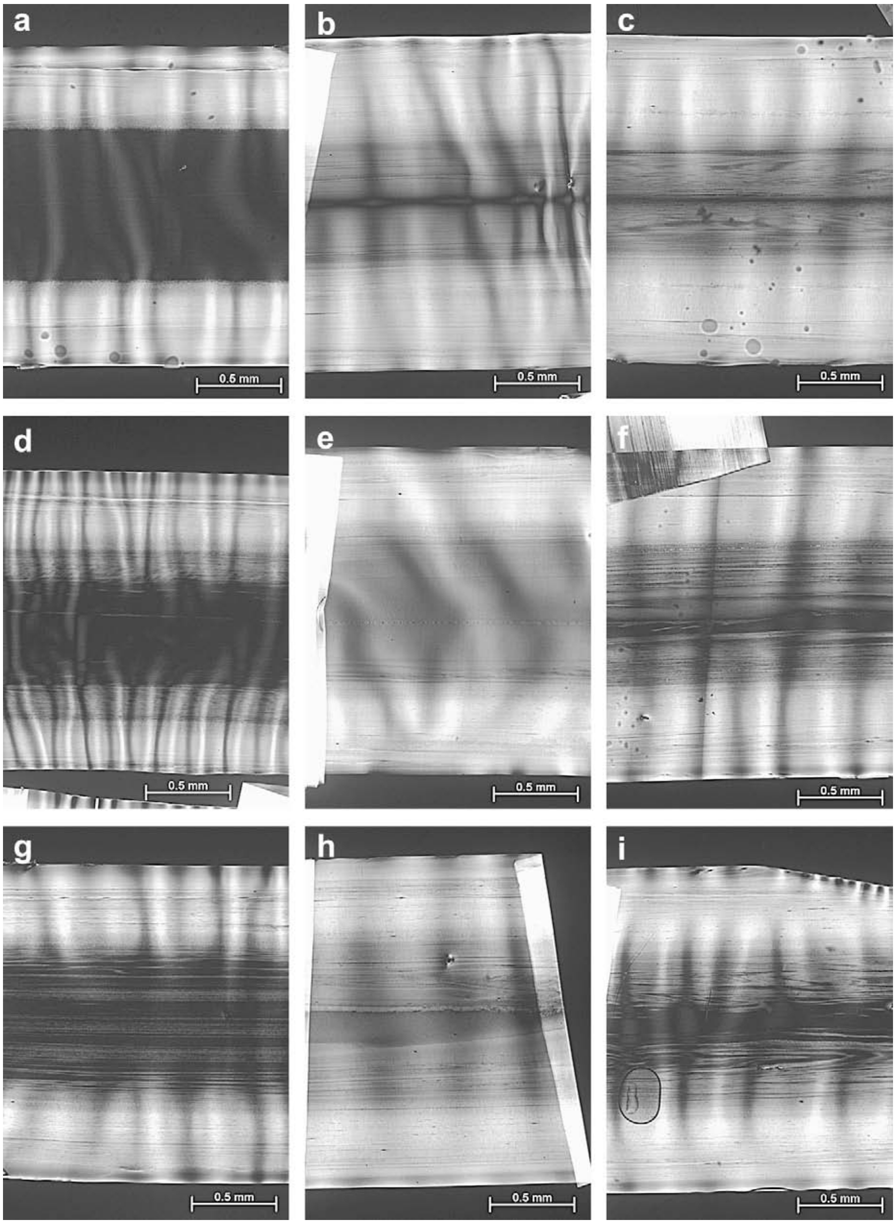

Fig. 8. Optical micrographs of cross-sections of samples of PP2_03 (a,b,c), PP2_07 (d,e,f) and PP2_10 (g,h,i) injection molded according to procedure A (a,d,g), B (b,e,h) and C (c, f, i), see Fig. 7.

$$L = \frac{2\pi}{q} \tag{4}$$

with λ the wavelength of the X-ray beam, d the distance between 2 crystal planes (WAXD) or the long period between 2 lamellae (SAXS, $d = L$), θ the scattering angle and q the scattering vector, defined as

$$q = \frac{4\pi \sin\ \theta}{\lambda} \tag{5}$$

The crystal lamellar thickness, l_c, is determined from:

$$l_c = LX_c \tag{6}$$

Under quiescent conditions, the lamellae grow from point nuclei in all directions, forming isotropic spherulitic structures, and the SAXS pattern shows an isotropic ring. For sufficiently strong flow conditions, molecules become oriented which crystallize into fiber-like structures that act as nuclei for the rest of the material. The remainder of the polymer grows onto these fibrils (shishes) creating parallel stacks of lamellae (kebabs). The structures are anisotropic which can be seen in SAXS as lobes in the flow direction. The extended chain crystals scatter, when enough present, showing streaks perpendicular to the flow direction. An extra feature that can be present in iPP is so-called lamellar branching, i.e. the parallel stacks of lamellae (mother) act as nuclei for crystals (daughter) that grow more or less perpendicular to the kebabs. In SAXS these daughter lamellae are observed as lobes in the same direction as the streaks.

Table 3
Values for the temperatures used in the experimental procedure displayed in Fig. 7.

DMDBS concentration [wt%]	$T_{\mathrm{ps,\,h}}$ [°C]	$T_{\mathrm{ps,\,c}}$ [°C]	T_2 [°C]	T_3 [°C]
0.3	180	164	160	175
0.7	210	187	185	200
1.0	215	193	190	210

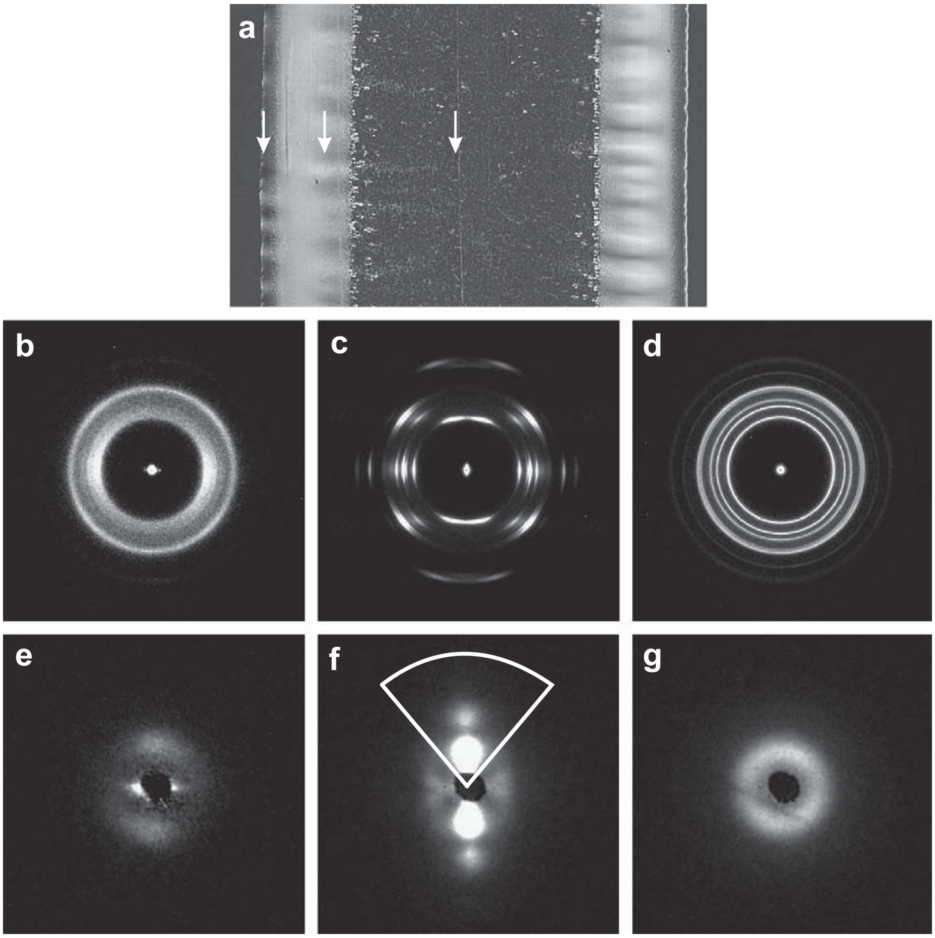

Fig. 9. (a) Optical micrograph of PP2 (40 mm s^{-1} for 2 s) with the arrows marking the spots of the X-ray patterns of the transition layer (b, e), the shear layer (c, f) and the core (d, g). Meridional integration area for SAXS is marked in (f).

2.7. Mechanical properties

Uniaxial tensile measurements are performed at a speed of 50 mm min^{-1}, which, with an initial length of the sample, $l_0 = 50$ mm, corresponds to a linear strain rate of 0.0167 s^{-1} up to a strain, ϵ, of 20% and the Young's modulus, E, and the strain at break, ϵ_b are determined.

3. Results and discussion

In the following the influence of different parameters in combination with varying processing conditions is presented.

3.1. Optical microscopy

3.1.1. Processing and MW

The morphology of injection molded samples is known to be inhomogeneous; up to 6 different layers were distinguished in injection molded PE samples, whose presence and thickness depend on the molding conditions applied and the position in the sample along the flow direction [62]. Fig. 3 shows the cross-sections of PP2 and PP3 produced with an injection speed of 40 mm s^{-1} for 2 s (Fig. 3(a) and (c)) and 5 mm s^{-1} for 16 s (Fig. 3(b) and (d)) to clarify the effect of molecular weight and processing conditions. Folding and buckling of the thin slices occur, due to stress relaxation after microtoming.

Layers that can be recognized from the edge to the core of the samples are a thin skin layer (A), a transition layer (B), a shear layer (C) and the isotropic core (D). The outer layer (A) is formed when the polymer melt comes in contact with the cold wall, and is cooled down rapidly to solidify. The transition layer (B) is formed on top of the skin layer, and is created by the flow front. Because of the thin skin layer, also the transition layer is cooled down rather rapidly. The melt traveling just next to the solid layer is sheared and the molecules get oriented. The shear layer (C) is created when these oriented chains crystallize. The molten polymer in the core (D) is only transported through the cavity deforming only mildly or not at all. The outer layers also have an insulating effect, i.e. the cooling rate in the core is low and the polymer only crystallizes after cessation of flow, allowing for chain relaxation, forming isotropic structures.

With lowering the injection speed both the thickness of the transition and shear layer increase at the expense of the core layer. During processing with a high injection speed (40 mm s^{-1}) the molecular deformation close to the wall of the mold is, almost from the start, high enough to orient and stretch the molecules. Here, close to the wall, the cooling rate is high and the stretched polymer chains crystallize forming the oriented shear layer right below the surface (Fig. 3(a)). On the other hand, a low injection speed is not strong enough to impose orientation to the molecules. The polymer forms isotropic structures during crystallization increasing the thickness of the transition layer. Thickening of the outer layer decreases the cross-section through which the melt still flows and hence, the shear stresses experienced increase and become strong enough to orient the polymer chains. The flow time is much higher (16 s versus 2 s) and thus, also the time the polymer melt

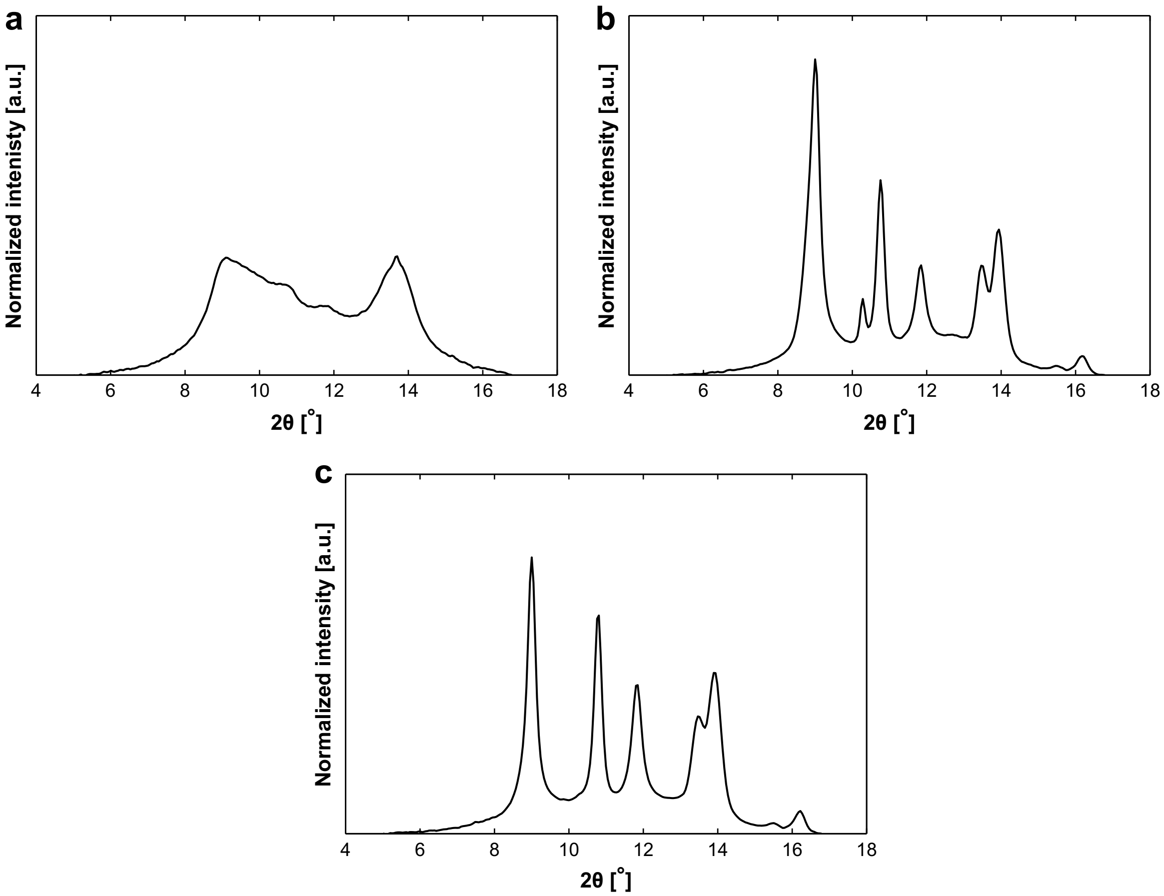

Fig. 10. 1D WAXD patterns of PP2 (40 mm s^{-1} for 2 s) of the transition layer (a), the shear layer (b) and the core (c).

experiences the shear stresses increases. During the flow period, the melt cools down more, the melt viscosity increases and relaxation times grow high, which leads to more pronounced orientation (Fig. 3(b)). The influence of melt viscosity is illustrated using PP3. This extrusion grade iPP has a higher molecular weight and melt viscosity forming a thicker oriented layer (Fig. 3(c)) [8,63]. At low shear rates, this layer even penetrates almost to the midplane of the sample (Fig. 3(d)).

The effect of processing conditions and molecular weight on the thickness of the shear layer is summarized in Fig. 4. For the high molecular weight (PP3) samples low injection speeds result in thick shear layers (thick because of the long flow times) covering almost the complete thickness of the mold. Especially at a change from 10 mm s^{-1} to 5 mm s^{-1} a sharp increase in shear layer thickness is observed. The lower molecular weight samples, PP1 and PP2, have a lower shear layer thickness and the increase in thickness is more gradual with decreasing injection speed.

3.1.2. *Processing and RaCos*

Fig. 4 also shows the effect of ethylene content on the shear layer thickness of samples injection molded with different speeds. It is observed that, similar to the lower molecular weights' pure iPP the shear layer thickness gradually increases with decreasing injection speed and slightly decreases with increasing ethylene content for all speeds applied. The molecular weight and weight distribution are the same for all four grades (see Table 1) and in an earlier study the linear visco-elastic behavior was determined which was shown to be equal in all cases [21]. The consequence of this is that under the same conditions, the melt viscosity and relaxation times change in a similar way and hence, the orientation of the molecules reaches the same level. The difference in shear layer thickness can be explained by the changed crystallization kinetics with increasing ethylene content. The addition of ethylene monomer restricts the formation of crystals because the ethylene does not match the PP crystal lattice and consequently, the crystallization temperature is lowered [64,65], requiring lower temperatures before crystallization sets in with the consequence that the shear layer does not penetrate the sample that far.

3.1.3. *Processing and DMDBS*

In Fig. 5 the cross-sections of PP2 and PP2_03 are compared. Differences observed are the absence of a transition layer in the PP2_03 sample and the absence of clear spherulitic structures in the core. The polymer crystallizes on top of the DMDBS fibrils, adopting the orientation of these fibrils. In contrast to the shear layers, in the core, they have a random orientation because phase separation occurred only after the flow was stopped (slow cooling in the core). The addition of DMDBS hardly changes the thickness of the oriented shear layer, where a strong orientational effect is expected [18].

Balzano et al. [18] studied the crystallization behavior of iPP-DMDBS systems by means of in situ X-ray measurements in a flow cell and concluded that the formation of a network of DMDBS fibrils, prior to application of flow, strongly influences the orientation of the resulting polymer structures. Flow simply orients the network of DMDBS fibrils and the crystals, growing on top, adopt this orientation. Kristiansen et al. [16] constructed the temperature/composition diagrams for cooling and heating of the iPP-DMDBS system. These phase diagrams are non-equilibrium in

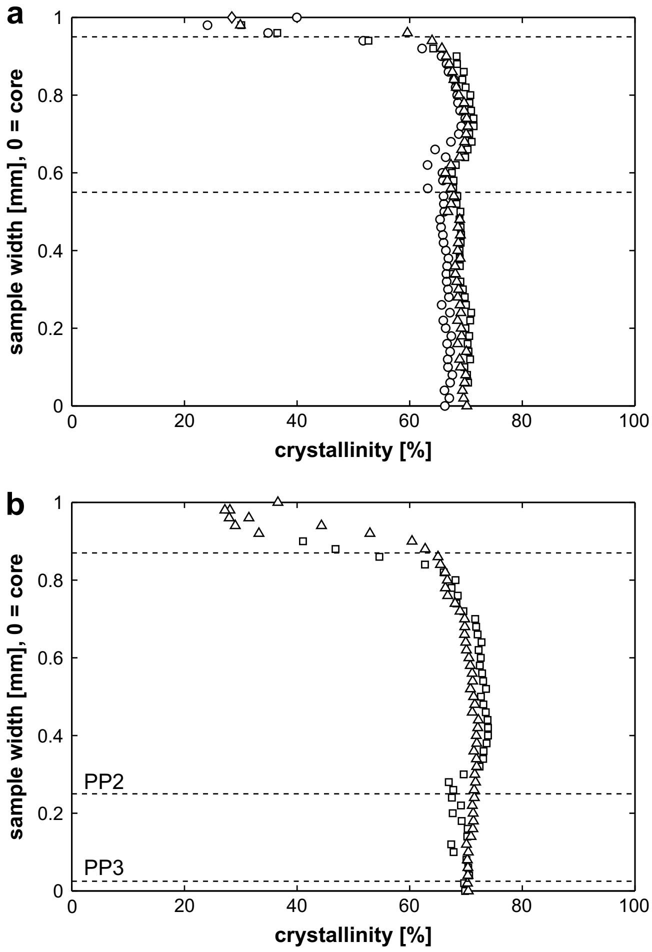

Fig. 11. Crystallinity, X_c, over the thickness of the sample processed with 40 mm s^{-1} for 2 s (a) and 5 mm s^{-1} for 16 s (△) (b): PP1 (○), only in (a), PP2 (□) and PP3 (△). Dashed lines indicate the position of the shear layer.

nature, and phase separation, upon cooling and dissolving of DMDBS in iPP during heating, occur at different temperatures. Similarly cooling rates have a large effect increasing the crystallization temperatures which went up 20 °C when lowering the cooling rate from 10 to 2 °C min^{-1}. We reconstruct the phase diagram using DSC and rheology applying heating and cooling rates of 10 °C min^{-1}, in the relevant concentration range of 0–1 wt%, see Fig. 6, and use this to interpret the results in Fig. 5.

At the start of the injection molding process DMDBS molecules are dissolved in the polymer melt and hence, flow cannot impose any orientation. During filling the mixture is cooled and phase separation starts but the time is too limited to form fibrils that can orient in flow. Phase separation occurs at a temperature of 165 °C only for a DMDBS concentration of 0.3 wt% (Fig. 6). For the higher concentrations of 0.7 wt% and 1.0 wt%, traces of oriented material are also found inside the core layer, see Fig. 8(d) and (g), respectively. This is explained by the higher phase separation temperatures, ~187 °C and ~193 °C, respectively, allowing DMDBS to form fibrils during filling that are oriented with flow.

3.1.4. *Processing after thermal treatment*

The phase diagram of iPP-DMDBS, Fig. 6, shows a temperature window in between the phase separation line upon cooling and dissolution line upon heating, where DMDBS fibrils survive, once formed. Via a thermal treatment of the melt, use can be made of this window, cooling first to allow for phase separation to occur and subsequent heating to produce highly oriented crystalline structures upon applying flow at temperatures, where normally flow has no influence on structure formation and isotropic morphologies are found [19]. The thermal treatment prior to injection consists of the following steps, see Fig. 7B:

- Melt polymer at $T_1 = 230$ °C.
- Cool to a temperature, T_2, just below $T_{ps,\ c}$ to form a DMDBS fibrillar network.
- Heat to a temperature, T_3, in between $T_{ps,\ c}$ and $T_{ps,\ h}$ to lower the melt viscosity. Here, the network is still intact.
- Inject the melt into mold.

with $T_{ps,\ c}$ and $T_{ps,\ h}$ the phase separation temperatures for the specific concentrations determined in a cooling (c) or heating (h) run, respectively. Experiment A is a standard injection molding, starting from T_1, and experiment C is a reference experiment in which the melt is cooled to T_3 without phase separation. The specific temperatures for the three DMDBS concentrations are found in Fig. 6 and listed in Table 3. The treatments are also applied to pure iPP2, to create another reference set, from which the structure distribution is investigated with WAXD and SAXS.

Fig. 8 shows cross-sections for the procedures A–C applied to all three DMDBS concentrations. It is observed that, in contrast to standard molding (A), treatment B shows almost complete orientation in the cross-section except for a small region in the core. The oriented layer is divided into two parts, the part at the edge shows high orientation (brightness) while closer to the core, a layer with lower brightness shows up. Unexpectedly, procedures B and C (without initial network formation) show only little differences. As mentioned, the phase diagram is not in equilibrium and the temperature of the transitions depend on the heating/cooling rate applied.

Lower cooling rates shift the transitions for both phase separation and crystallization to higher temperature. Since the barrel is not actively cooled the resulting cooling rates are low and it could be, that, instead of what is assumed, the reference experiment C also starts with a fibrillar network present. This is even more likely, since the temperature T_3 lies just above the phase separation temperature $T_{ps,\ c}$, and therefore only few degrees of cooling are needed before DMDBS fibrils start to form. This might occur during the filling stage, enabling flow to orient fibrils also in case of experiment C. Another explanation for the lack of difference between B and C, at least as observed in OM, is 'flow induced phase separation' [18], which causes an immediate crystallization of DMDBS at flow just above the phase separation temperature. For the two other concentrations, the same observations are made and using protocol B, fully oriented samples are obtained. The differences between the procedures B and C are more pronounced now. The B samples have a fully oriented core with an even brightness between crossed polars, while the C samples show center regions with isotropic structures is present, while the low oriented layer at some distance from the edge has a less homogeneous appearance, represented by alternating light and dark sequences.

3.2. *Structural properties from WAXD/SAXS*

Because of the symmetry only half of the thickness is used for the X-ray analysis. Fig. 9 shows the 2D X-ray patterns corrected for background scattering (flow direction is vertical) for the different layers found over the thickness in PP2 molded with at a speed of 40 mm s^{-1} for 2 s. The measuring positions are marked by the arrows in Fig. 9(a). Although 4 layers are distinguished in the optical micrographs of Fig. 3, the outer skin layer is too thin to be

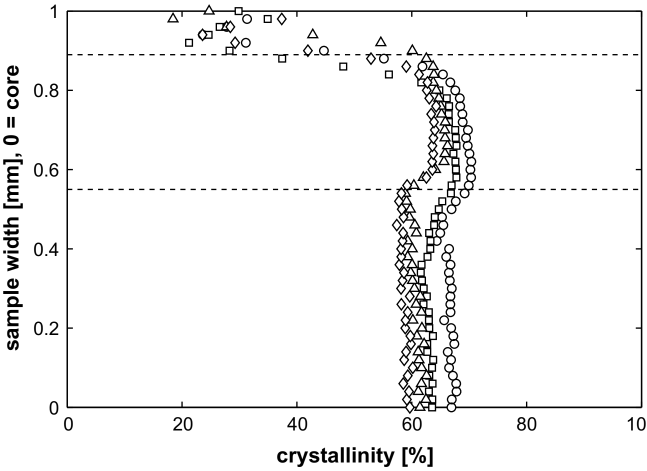

Fig. 12. Crystallinity, X_c, over the thickness of the sample for PP1 (○) and RACO1 (□), RACO2 (△) and RACO3 (◇) processed with 20 mm s^{-1} for 4 s. Dashed lines indicate the position of the shear layer.

detected with the X-ray beam, and only severe edge scattering is observed. The transition layer consists almost completely of mesomorphic crystals right next to the skin layer, shown by two broad rings in Fig. 9(b). At this position, the polymer is quenched and has no time to form well-defined crystal structures. Approaching the shear layer, the mesomorphic phase diminishes and scattering peaks of α-phase crystals appear combined with strong arcing of the Debye–Scherrer rings, indicating that the crystalline morphology is oriented in flow direction, Fig. 9(c). Not only α-phase crystals are present, also traces of β-phase crystals are observed. The structures in the core are isotropic, see Fig. 9(d), and consists completely of the α-phase. Scattering at small angles (SAXS) in the center of the WAXD patterns is depicted in Fig. 9(e)–(g). In the transition layer, they show streaks at the equator from shishes oriented in flow, and a broad ring, slightly oriented, indicating that the lamellar thickness is distributed broadly, Fig. 9(e). The pattern of the shear layer, Fig. 9(f), contains all the features of anisotropic structures: (i) lobes on the meridian arising from stacks of parallel lamellae, (ii) streaks at the equator, although vague, from the shishes oriented in flow, and (iii) lobes at the equator from daughter lamellae growing approximately perpendicular to the mother lamellae. Furthermore, the double lobes on the meridian, which is second order scattering, indicate that the periodicity of the lamellae is high [66]. The core pattern is an isotropic ring, which means that lamellae grow in all directions, Fig. 9(g).

The 1D WAXD patterns, obtained by circular integration, are presented in Fig. 10. The intensity is normalized by defining the total area equal to one. In these graphs the peak positions are recognized easier (Table 2). A small amount of α-phase structures is already formed next to the edge in the transition layer, see Fig. 10(a), while in the shear layer reveals that, next to the α and

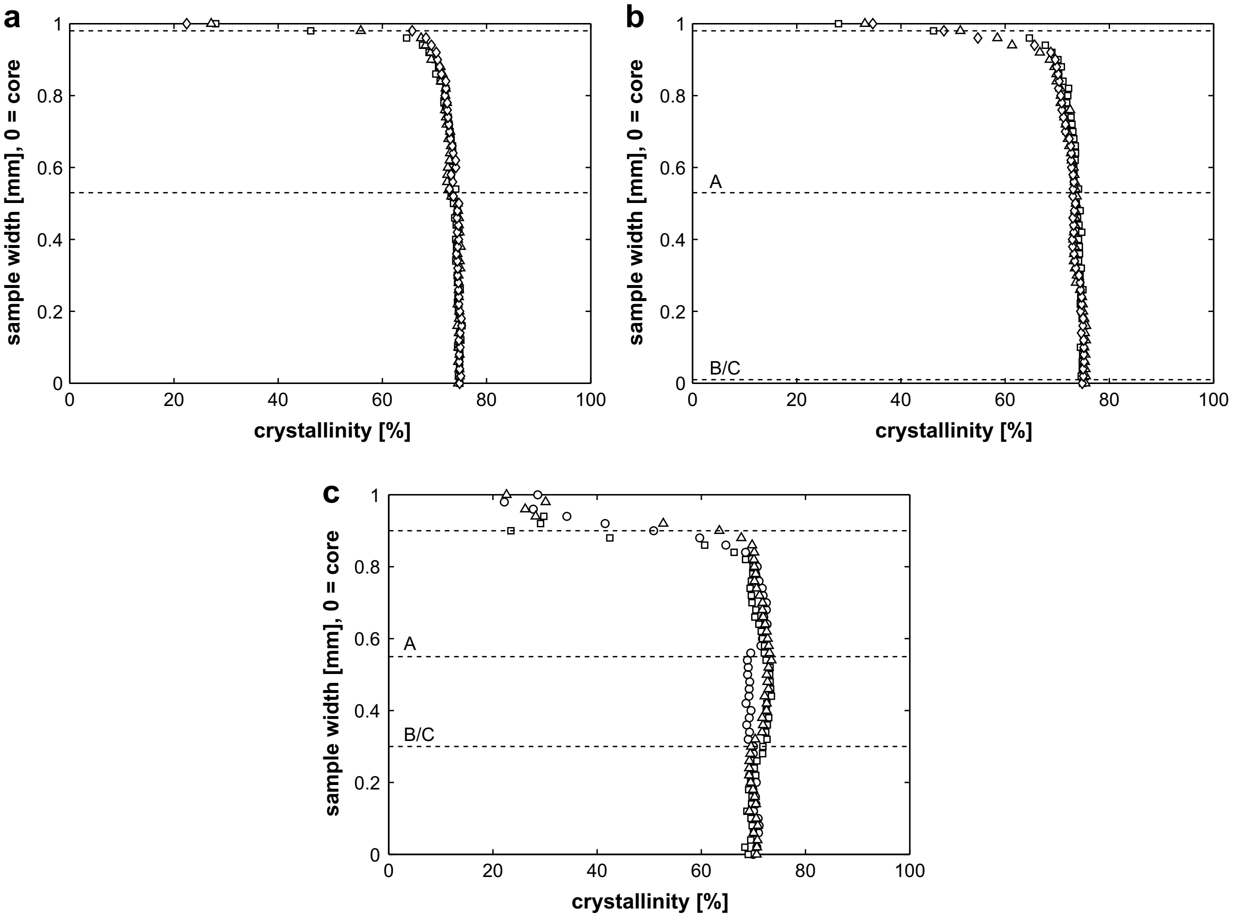

Fig. 13. Crystallinity, X_c, over the thickness of the sample: (a) experiment A for the blends PP2_03 (□), PP2_07 (△) and PP2_10 (◇) (b) experiment A (□), experiment B (△) and experiment C (◇) for blend PP2_03 and (c) the corresponding pure PP2 reference samples. Dashed lines indicate the position of the shear layer.

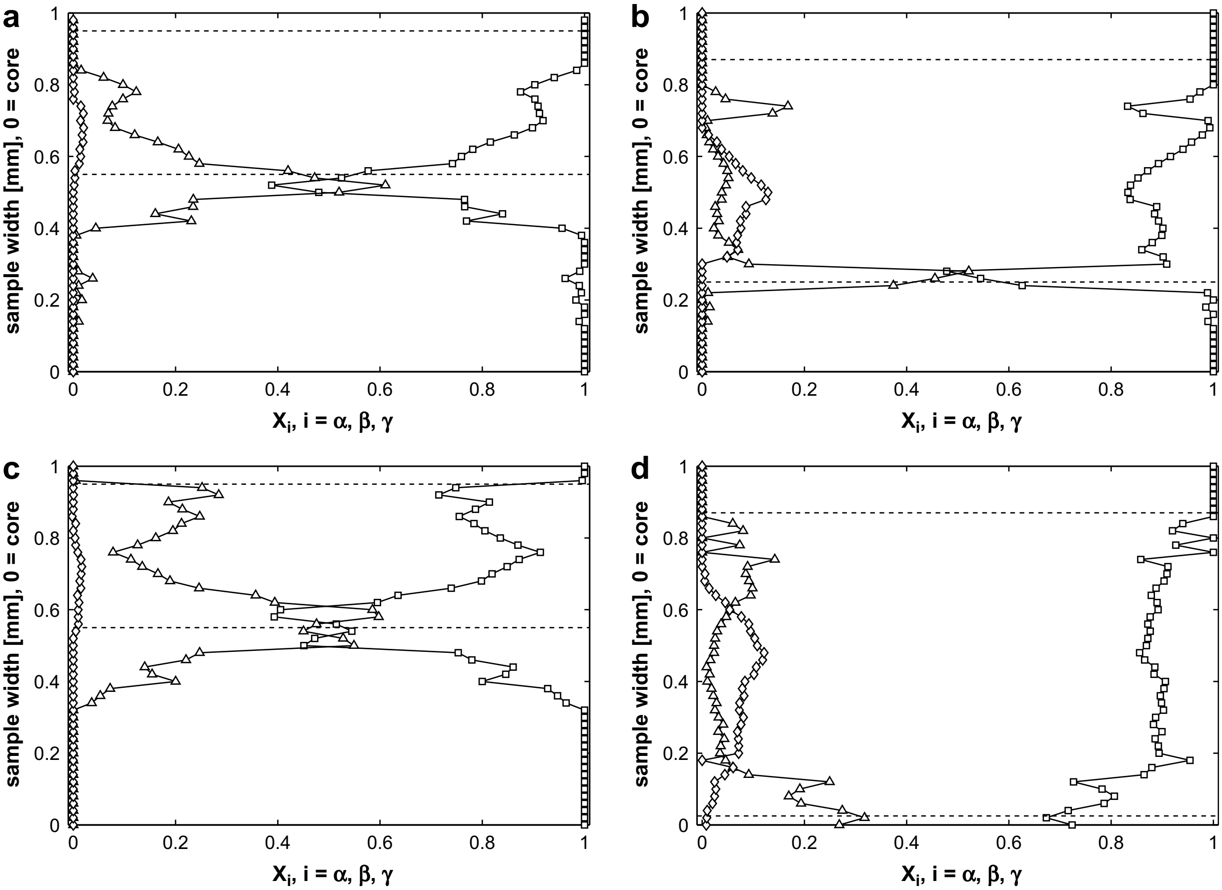

Fig. 14. Fraction of specific crystal phase, X_i with i = α (□), β (△) or γ (◇), over the thickness of the sample of PP2 (a, b) and PP3 (c, d): 40 mm s^{-1}, 2 s (a, c) and 5 mm s^{-1}, 16 s (b, d). Dashed lines indicate the position of the shear layer.

β-phase, also some γ crystals are present. In the next sections, further analysis and quantification of structural characteristics, like crystallinity, will be presented.

3.2.1. Crystallinity

The 1D WAXD patterns are used to determine crystallinity with equation (1). The amorphous halo has been scaled as shown in Fig. 2(a), which is valid as long as no structures of the β-type form. When β-phase crystals arise, a diffraction peak appears at an angle of $2\theta = 10.26^\circ$ in between the $(110)_\alpha$ and $(140)_\alpha$ peaks, causing the amorphous part to be overestimated, which will bring the value of crystallinity down. To compensate for this, an average amorphous halo is calculated from all patterns which did not show any traces of β crystals. These regions include the complete core and some parts from the transition and shear layer, and the amorphous halo proves to be more or less the same at every measurement position. For the neat polymers, processed with a speed of 40 mm s^{-1} for 2 s, and 5 mm s^{-1} for 16 s, crystallinity is plotted as a function of position in Fig. 11. The crystallinity in the core is almost constant for all three grades, at both conditions, and has a value of approximately 69%. At the edge of the samples, X_c is lower, because of the high cooling rates experienced, resulting in the formation of mesomorphic phase with a low crystalline order. In the shear layer, the values for X_c are a few percent higher than in the core layer. It shows that a change in processing conditions, injection speed and time, does not effect the overall crystallinity of the samples.

Fig. 12 shows the crystallinity distribution for PP1, RACO1, RACO2 and RACO3 (20 mm s^{-1}, 4 s). The incorporation of ethylene monomer decreases of crystallinity [20,21], because it restricts the formation of crystals since ethylene does not match the PP crystal lattice [64,65]. The addition of DMDBS changes the crystallinity profile only slightly, Fig. 13, and an almost constant crystallinity from edge to core is found with an average $X_c = 74\%$. No difference is observed for an increased amount of nucleating agent, Fig. 13(a), neither for procedure B, performed to induce orientation, and C, the reference experiment, Fig. 13(b). The reference samples of pure PP2, with thermal treatments B and C, show no change in crystallinity compared to procedure A, Fig. 13(c), only the thickness of the shear layer, in which X_c is higher than in the isotropic core, is increased [63].

3.2.2. Polymorphism

Polypropylene can form different types of crystals depending on the crystallization conditions. It was proposed by Corradini et al. [61] that the mesomorphic phase is similar to an α phase with a short range order, but here we will disregard the mesomorphic phase, because it only appears at severe cooling conditions which is only achieved in a thin layer close to the wall. When going from the edge to the core, the amount of mesomorphic crystals decreases rapidly (<0.1 mm) and the two broad peaks are overgrown by peaks of the other crystal phases, making them almost impossible to distinguish. Fig. 14(a)–(d) shows the distribution of the fractions of the three different phases (α, β, γ) over the thickness of the samples of PP2 and PP3, prepared with an injection speed of 40 mm s^{-1} for 2 s, and 5 mm s^{-1} for 16 s. When comparing the results the following can be observed:

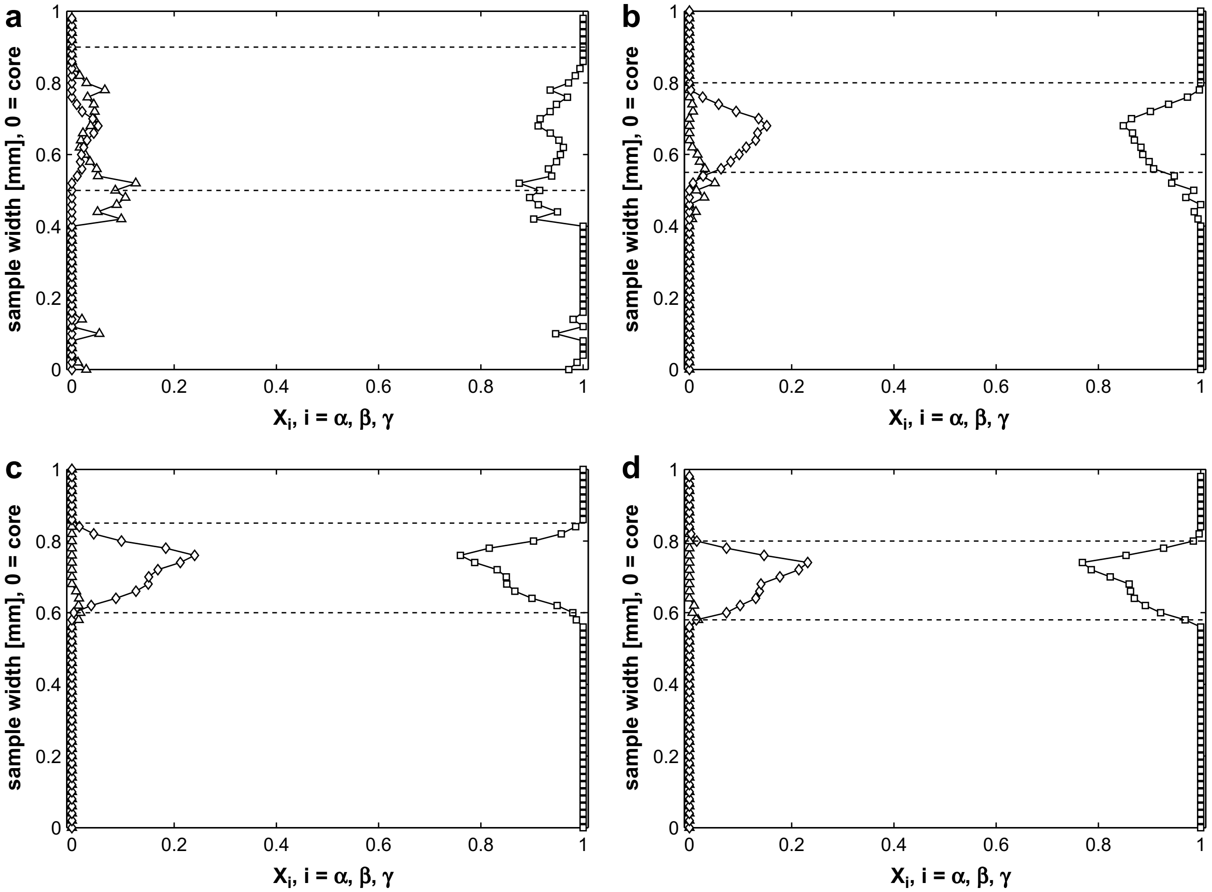

Fig. 15. Fraction of specific crystal phase, X_i with i = α (□), β (△) or γ (◇), over the thickness of sample PP1 (a), RACO1 (b), RACO2 (c) and RACO3 (d). Dashed lines indicate the position of the shear layer.

- The core consists solely of α crystals independent of the processing conditions or molecular weight.
- Only in the shear layer other crystal forms are present.
- Within the shear layer, the amount of β crystals increases towards the core, with its maximum at the transition from shear layer to core.
- With decreasing injection speed, the maximum amount of β crystals decreases slightly.
- An increase in molecular weight does not alter the maximum amount of β crystals.
- At the high injection speed, only a few percent γ crystals is present, increasing with decreasing injection speed.
- The amount of γ crystals is unaffected by molecular weight.

The maximum fraction of β phase crystals is found at the transition between the shear layer and the core, because here, the strongest orientation is imposed by flow [44–46]. Due to flow, which orients chains, the polymer crystallizes at a higher temperatures where the γ phase is more stable than the α phase [52].

The presence of ethylene monomer changes the distribution of crystal phases, see Fig. 15(a)–(d). The amount of β phase strongly decreases with increasing amount of ethylene to almost 0% for RACO3 [67], while in the shear layer a strong increase in γ phase crystals observed. Given the same thermal history for all samples, this means that an increasing ethylene content broadens the temperature range in which the γ phase occurs shifting it to lower temperatures [52].

Fig. 16(a)–(c) shows the crystal type distribution over the thickness of a PP2_03 sample prepared according to procedures A, B and C, respectively. Compared to the neat polymer, two differences can be detected:

- The core does not solely consists of α, but also of a noticeable amount of γ crystals ranging from 0% near the shear layer to 5–10% in the center.
- Within the shear layer, the amount of β crystals is decreased strongly by order 4.

The DMDBS concentration has no further influence on the amount and distribution of crystal phases, see Fig. 16(d), for the sample containing 0.7 wt% DMDBS. The polymer crystallizes at higher temperatures due to the nucleating agent, which is closer to the stable γ phase region increasing γ crystal formation. The creation of β phase is suppressed, because DMDBS is an α nucleating agent. The X-ray results show that, despite the clear differences when observed under a microscope (Fig. 8), crystal (type) formation is dictated by the presence of DMDBS. For the pure iPP the treatments A–C have a considerable consequence for the crystal phase distribution and with decreasing the initial melt temperature, the amount of α phase increases at the expense of the β phase, see Fig. 17.

3.2.3. Lamellar thickness

To determine lamellar thickness from SAXS, the 2D patterns are circularly integrated around the meridian, see Fig. 9(f), to avoid disturbance of the equatorial region where, in case of orientation,

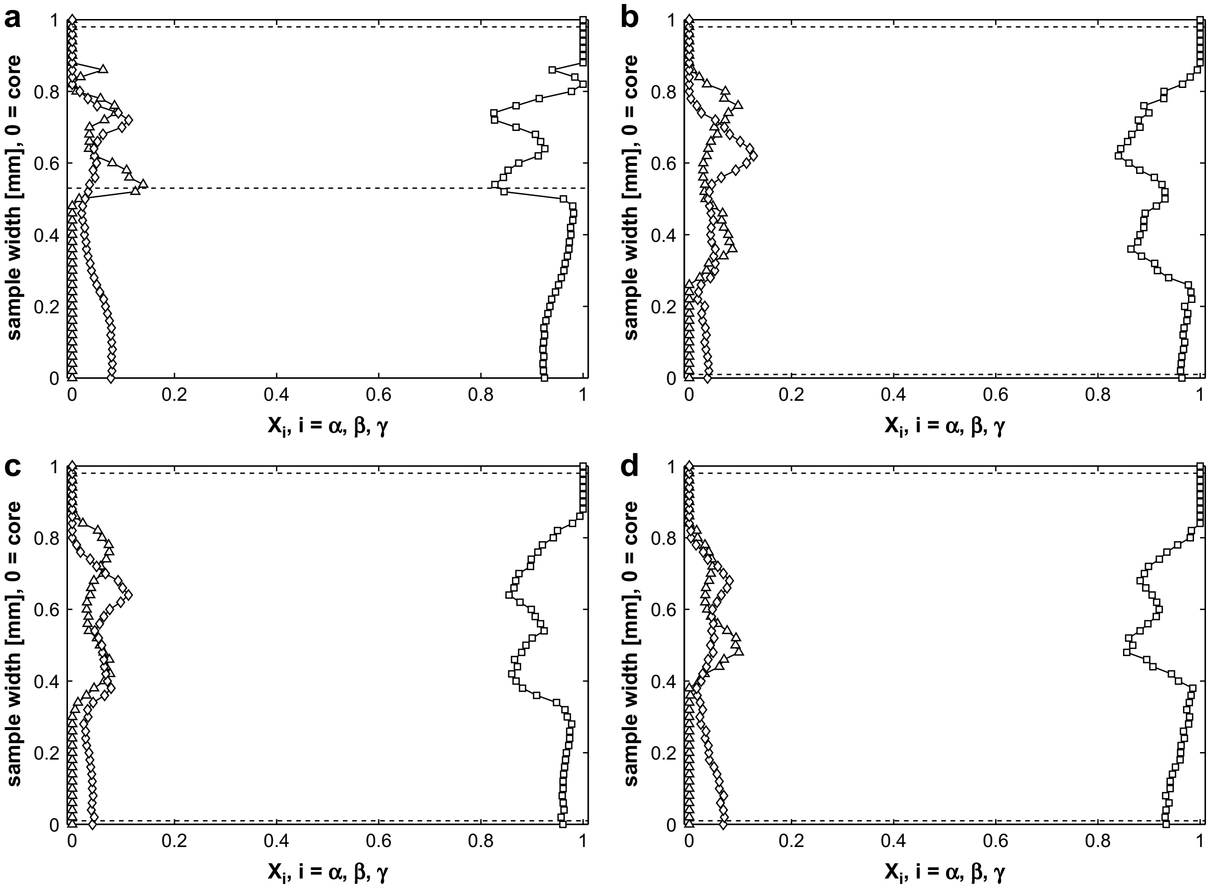

Fig. 16. Fraction of specific crystal phase, X_i with i = α (□), β (△) or γ (◇), over the thickness of sample PP2_03, experiment A (a), experiment B (b) and experiment C (c), and experiment C of sample PP2_07 (d). Dashed lines indicate the position of the shear layer.

streaks arise from scattering of shishes. In case of isotropic orientation the lamellar thickness is the same in all directions as are the results from both meridional integration and full integration. For an anisotropic morphology, this method gives the thickness of the oriented lamellae, which, in most cases, dominates the thickness distribution and only few lamellae are isotropically distributed, i.e. only a small amount of spherulites are present. The long period is at $q = q_{I_{\max}}$, the q-value corresponding to the maximum in scattered intensity, $I_{\max}$.

Fig. 18 shows the lamellar thickness, l_c, for the PP1, PP2 and PP3 samples as depicted in Figs. 3, 11 and 14. In all cases, l_c increases, starting at a low value at the wall, where time to form crystallites is small, to a maximum in the shear layer, after which it decreases to a constant value of ∼10 nm in the core layer. Flow orients (and stretches) polymer chains, as such decreasing the entropy of the system and the material crystallizes at higher temperatures resulting in thicker lamellae in the shear layer. In the core, the polymer crystallizes after cessation of flow under quiescent

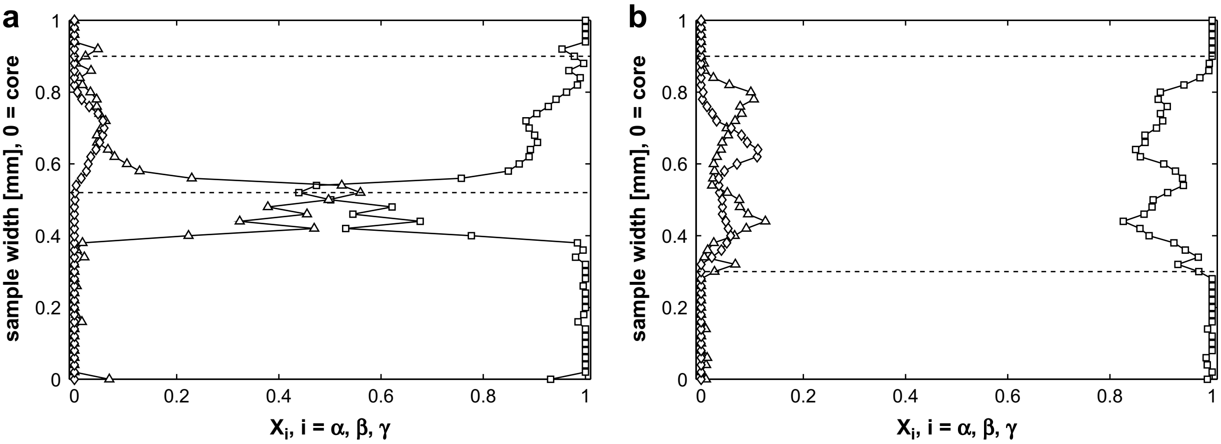

Fig. 17. Fraction of specific crystal phase, X_i with i = α (□), β (△) or γ (◇), over the thickness of sample PP2 (20 mm s^{-1}, 4 s), experiment A (a) and experiment C (b). Dashed lines indicate the position of the shear layer.

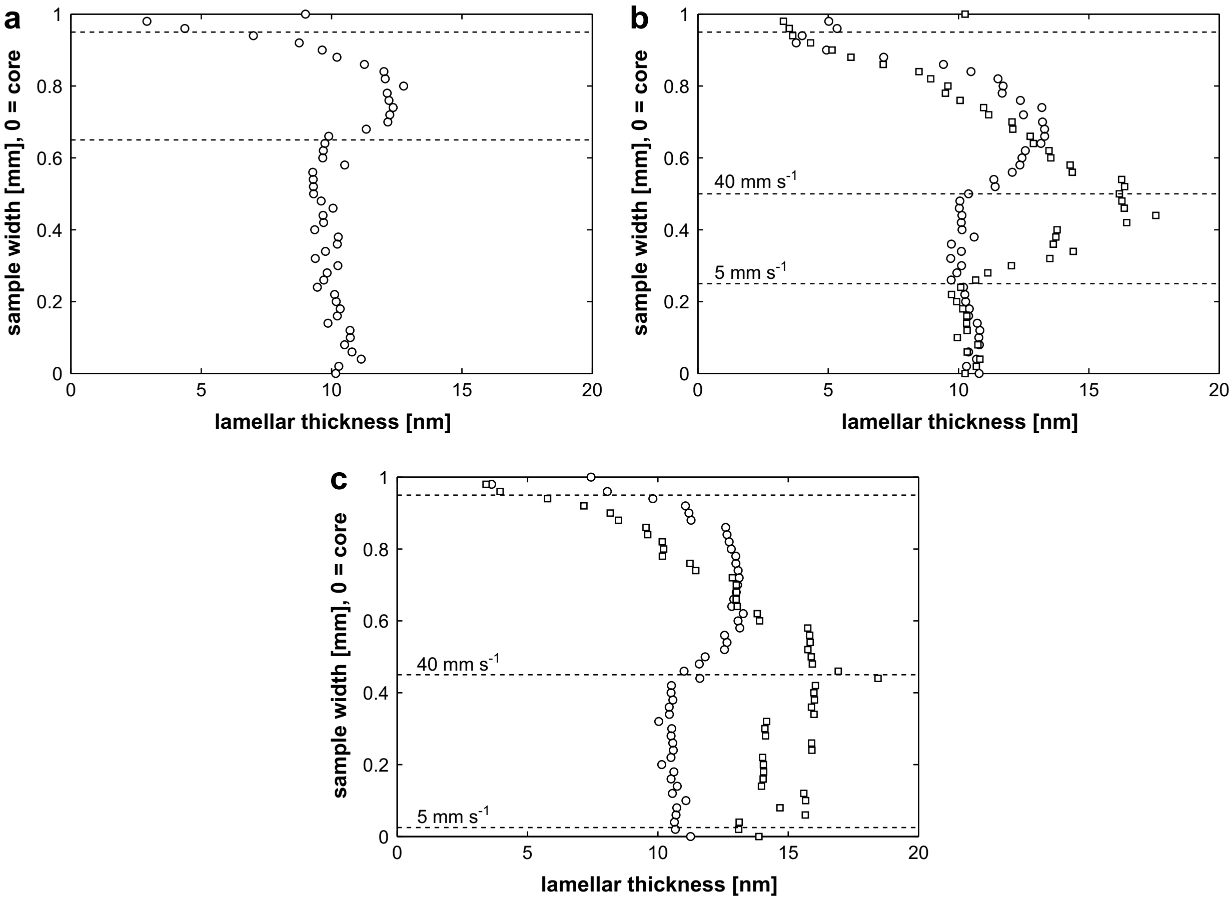

Fig. 18. Crystal lamellar thickness, l_c, over the thickness of PP1 (a), PP2 (b) and PP3 (c): 40 mm s^{-1} for 2 s (○), 5 mm s^{-1} for 16 s (□). Dashed lines indicate the position of the shear layer.

conditions at the same temperature, lower than in the shear layer, and the lamellar thickness is constant. The increase of l_c from the wall is faster for the samples processed at a high injection speed; stronger orientation of polymer chains and a larger decrease in entropy, results in higher temperature at which the polymer crystallizes and hence, thicker lamellae at the same sample position. The higher maximum lamellar thickness for the low injection speed is a result of the longer shear time, during which the melt is cooled, the chains are oriented and stretched strongly, i.e. more than in the high speed samples, and the lamellae are created at even higher temperatures.

For an increase in ethylene content, a decrease of lamellar thickness over the full sample width is observed, see Fig. 19, caused by crystallization at lower temperatures.

For the nucleated samples, similar to the results of crystallinity and crystal phase (Figs. 13 and 16) the lamellar thickness becomes constant over the thickness, independent of concentration DMDBS and thermal treatment applied, see for example Fig. 20(a) for PP2_03. This shows, that DMDBS dictates the crystallization process, i.e. only the presence of DMDBS, which forms the fibrillar nuclei during cooling, determines at which temperature iPP crystallizes and flow, which orients the fibrils, does not increase the crystallization temperature, thus l_c is constant. The reference samples of PP2 on the other hand, which got the same thermal treatments, do show an effect of thermal treatment on the distribution of lamellar thickness, see Fig. 20(b). The shear layer becomes almost twice as thick, in which l_c is constant (~14 nm). To summarize the comparison between pure iPP and the iPP-DMDBS samples:

- DMDBS dictates the morphology distribution (X_c, crystal phases and l_c) independent of thermal treatment, only the oriented shear layer thickness increases.
- The reference samples of PP2 also show a thickness increase of the shear layer when thermally treated, in which X_c and l_c are higher than in the core layer and the distribution of crystal phases is changed.

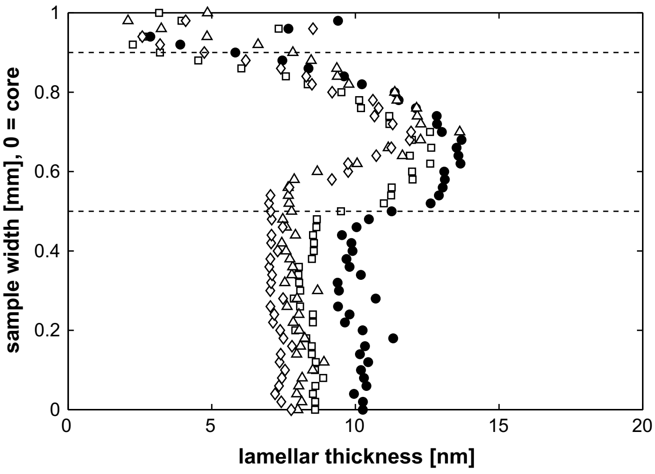

Fig. 19. Crystal lamellar thickness, l_c, over the thickness of PP1 (●), RACO1 (□), RACO2 (△) and RACO3 (◇), processed with 20 mm s^{-1} for 4 s. Dashed lines indicate the position of the shear layer.

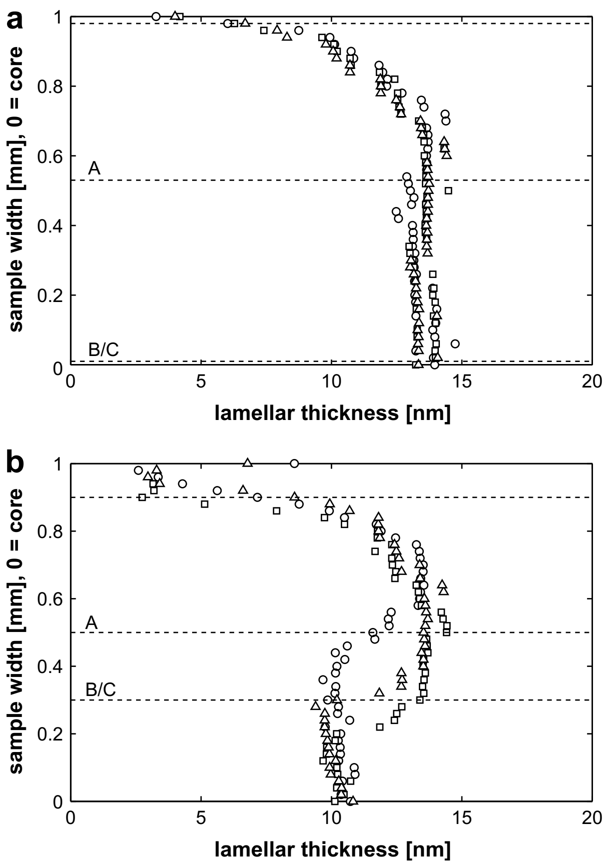

Fig. 20. Crystal lamellar thickness, l_c, over the thickness of PP2_03 (a) and PP2 (b): procedure A (○), procedure B (□) and procedure C (△), processed with 20 mm s^{-1} for 4 s. Dashed lines indicate the position of the shear layer.

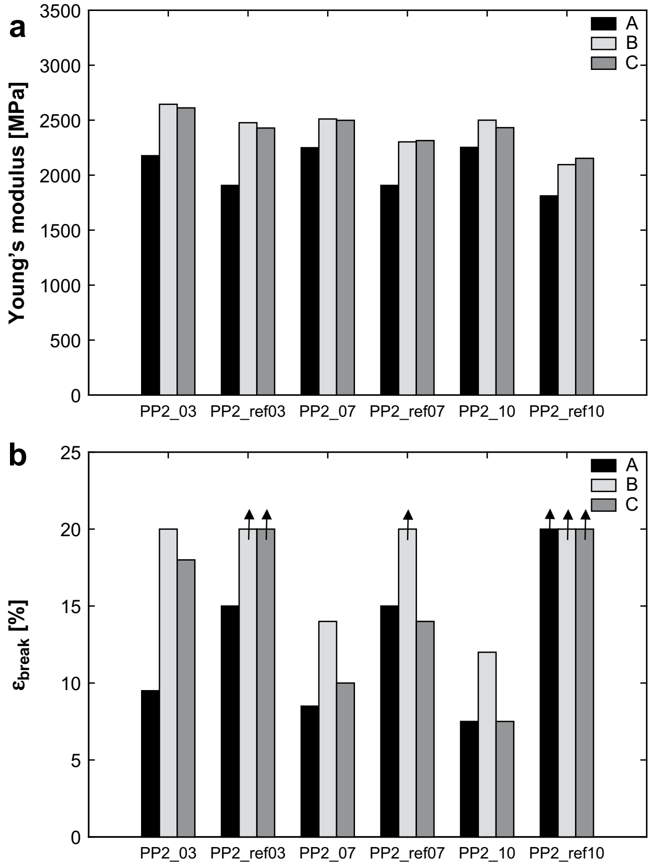

Fig. 21. Young's modulus (a) and strain at break, ϵ_{break} (b), of all iPP-DMDBS samples and their corresponding PP2 reference samples for procedures A, B and C. The arrows in (b) indicate that the samples did not break at the maximum applied strain of 20%.

3.3. Mechanical properties

Fig. 21 shows the Young's modulus and strain at break, ϵ_{break}, obtained for all samples. The standard molded samples, A, show that the addition of DMDBS leads (i) to an increase in Young's modulus and (ii) to a decrease in ϵ_{break}, implying that the toughness decreases. For all samples, with and without DMDBS, a thermal treatment prior to injection, B, improves the properties measured in flow direction. The difference in the Young's modulus is minor, 20% for 0.3 wt% DMDBS down to ~10% for 1.0 wt%, but a profound difference in toughness is obtained. Some samples did not break at the maximum strain applied of 20%, which is indicated by the arrows in Fig. 21(b).

In the samples containing DMDBS no influence of concentration and experimental procedure is found on X_c, crystal phases and l_c, only the shear layer penetrates further into the sample. The last was also observed in the reference samples, where the distribution of X_c, crystal phases and l_c was indeed influenced. Pukánsky et al. [68] showed that a correlation exists between the crystallization temperature, thus the lamellar thickness, l_c, and the modulus. A special structural feature, observed in polymer samples formed under high pressure and in specially drawn fibers, is the so-called zip-fastener structure, in which tapered lamellae, grown from extended chains in close proximity, interlock [69–72]. Interpenetration of lamellae improves transfer of load between the structures with, as a result, sometimes extreme increase in modulus [69–71]. It is suggested that this structure also improves the toughness. In our samples (partial) interlocking of kebabs is present in the thick shear layers that contain oriented structures with a fibrillar core, either DMDBS fibrils or iPP shishes, overgrown by lamellae. Fig. 22 shows the integrated SAXS pattern of PP2_03, procedure B, at a position in the shear layer, which represents the distribution of lamellar thicknesses. The distribution is dominated by thick lamellae as seen from the peak at low q-values, but the thicknesses are widespread, which might indicate the presence of interlocked, tapered lamellae [69].

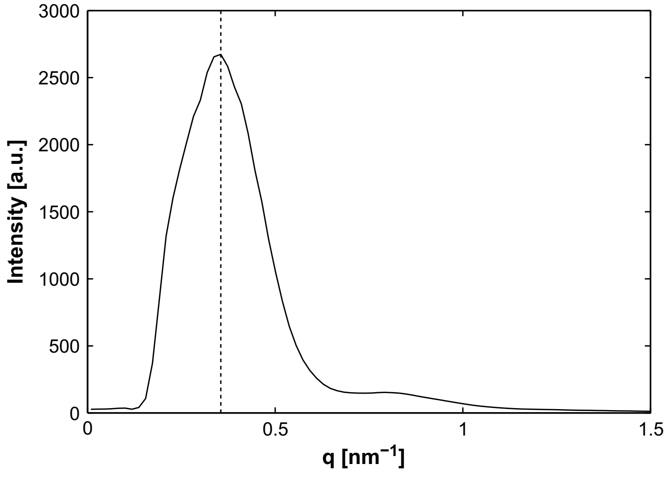

Fig. 22. Integrated SAXS pattern of PP2_03, procedure C, near the core, showing the distribution of lamellar thicknesses.

4. Conclusions

The morphology distribution in injection molded polypropylene samples is characterized using optical microscopy and X-ray diffraction. The influences of molecular weight and its distribution, of a change in chain composition and of nucleating agents are investigated. Several structural layers are found with a different level of orientation. The thickness of the oriented shear layer decreases with decreasing MW and MWD, and with an increasing amount of ethylene monomer, for the same processing conditions, while the addition of DMDBS hardly influences the layer thickness, but increases the uniformity of the structural features in the layers. The layers contain different structural objects (spherulites, shish-kebabs), resulting in changes in structural features, i.e. crystallinity, the type and amount of crystal phase and lamellar thickness. A thermal treatment prior to injection, based on the phase diagram of the iPP-DMDBS system, leads to an oriented morphology over the full width of the samples, without changing X_c, crystal phases and l_c. All thermally treated samples, including those without DMDBS, show a considerable improvement in mechanical properties.

Acknowledgements

This work is part of the Research Programme of the Dutch Polymer Institute (DPI), P.O. Box 902, 5600 AX Eindhoven, The Netherlands, project no. #454.

References

[1] Gahleitner M, Wolfschwenger J, Bachner C, Bernreitner K, Neissl W. Journal of Applied Polymer Science 1996;61:649–57.
[2] Lagasse RR, Maxwell B. Polymer Engineering and Science 1976;16:189–99.
[3] Keller A, Kolnaar HWH. Flow induced orientation and structure formation. In: Meijer HEH, editor. Processing of polymers, vol. 18. New York: VCH; 1997. p. 189–268.
[4] Vleeshouwers S, Meijer HEH. Rheologica Acta 1996;35:391–9.
[5] Somani RH, Hsiao BS, Nogales A, Srinivas S, Tsou AH, Sics I, et al. Macromolecules 2000;33:9385–94.
[6] Seki M, Thurman DW, Oberhauser JP, Kornfield JA. Macromolecules 2002;35:2583–94.
[7] Vega JF, Hristova DG, Peters GWM. Journal of Thermal Analysis and Calorimetry, special issue, in press.
[8] Liedauer S, Eder G, Janeschitz-Kriegl H, Jerschow P, Geymayer W, Ingolic E. International Polymer Processing 1993;VIII:236–44.
[9] Kumaraswamy G, Issaian AM, Kornfield JA. Macromolecules 1999;32:7537–47.
[10] Kumuraswamy G, Verma RK, Issaian AM, Wang P, Kornfield JA, Yeh F, et al. Polymer 2000;41:8931–40.
[11] Baert J, Van Puyvelde P. Polymer 2006;47:5871–9.
[12] Baert J, Van Puyvelde P, Langouche F. Macromolecules 2006;39:9215–22.
[13] Schrauwen BAG. Ph.D. thesis, Eindhoven University of Technology, The Netherlands; 2003.
[14] Muratoglu OK, Argon AS, Cohen RE, Weinberg M. Polymer 1995;36:921–30.
[15] Ergungor Z, Cakmak M, Batur C. Macromolecular Symposia 2002;185:259–76.
[16] Kristiansen M, Werner M, Tervoort T, Smith P, Blomenhofer M, Schmidt HW. Macromolecules 2003;36:5150–6.
[17] Kristiansen M, Tervoort T, Smith P, Goossens H. Macromolecules 2005;38:10461–5.
[18] Balzano L, Rastogi S, Peters GWM. Macromolecules 2008;41:399–408.
[19] Balzano L, Portale G, Peters GWM, Rastogi S. Macromolecules 2008;41:5350–5.
[20] Gahleitner M, Jääskeläinen P, Ratajski E, Paulik C, Reussner J, Wolfschwenger J, et al. Journal of Applied Polymer Science 2005;95:1073–81.
[21] Housmans JW, Peters GWM, Meijer HEH. Journal of Thermal Analysis and Calorimetry, special issue, in press.
[22] Yalcin B, Cakmak M. Polymer 2004;45:2691–710.
[23] US Patent 133229, Patented November 19, 1872.
[24] Custodio FJMF. Ph.D. thesis, Eindhoven University of Technology, The Netherlands; 2009.
[25] Custodio FJMF. PhD Thesis. Eindhoven University of Technology, The Netherlands; 2009.
[26] Thierry A, Fillon B, Straupé C, Lotz B, Wittmann JC. Progress in Colloid and Polymer Science 1992;87:28–31.
[27] Shepard TA, Delsorbo CR, Louth RM, Walborn JL, Norman DA, Harvey NG, et al. Journal of Polymer Science, Part B: Polymer Physics 1997;35:2617–28.
[28] Swartjes FHM. Ph.D. thesis, Eindhoven University of Technology, The Netherlands; 2001.
[29] Swartjes FHM, Peters GWM, Rastogi S, Meijer HEH. International Polymer Processing 2003;XVIII:53–66.
[30] van der Beek MHE. PhD Thesis, Eindhoven University of Technology, The Netherlands; 2005.
[31] van der Beek MHE, Peters GWM, Meijer HEH. International Polymer Processing 2005;XX:111–20.
[32] van der Beek MHE, Peters GWM, Meijer HEH. Macromolecules 2006;39:1805–14.
[33] van der Beek MHE, Peters GWM, Meijer HEH. Macromolecules 2006;39:9278–84.
[34] Forstner R, Rendina C, Housmans JW, Peters GWM, Meijer HEH. Journal of Thermal Analysis and Calorimetry, special issue, in press.
[35] Housmans JW. PhD Thesis. Eindhoven University of Technology, The Netherlands; 2008.
[36] Zuidema H, Peters GWM, Meijer HEH. Macromolecular Theory and Simulations 2001;10:447–60.
[37] Zuidema H, Peters GWM, Meijer HEH. Journal of Applied Polymer Science 2001;82:1170–86.
[38] Ulcer Y, Cakmak M, Miao J, Hsiung CM. Journal of Applied Polymner Science 1996;60:669–91.
[39] van de Burgt FPTJ, Rastogi S, Chadwick JC, Rieger B. Journal of Macromolecular Science, Part B; Physics 2002;B41:1091–104.
[40] van der Burgt FPTJ. PhD Thesis, Eindhoven University of Technology, The Netherlands; 2002.
[41] Norton DR, Keller A. Polymer 1985;26:704–16.
[42] Lotz B, Wittmann JC. Journal of Polymer Science, Part B; Polymer Physics 1986;24:1541–58.
[43] Lovinger AJ, Chua JO, Gryte CC. Journal of Polymer Science Polymer Physics Edition 1977;15:641–56.
[44] Varga J, Karger-Kocsis J. Polymer Bulletin 1993;30:105–10.
[45] Varga J, Karger-Kocsis J. Journal of Polymer Science, Part B: Polymer Physics 1996;34:657–70.
[46] Jay F, Haudin JM, Monasse B. Journal of Materials Science 1999;34:2089–102.
[47] Varga J, Mudra I, Ehrenstein GW. Journal of Applied Polymer Science 1999;74:2357–68.
[48] Mathieu C, Thierry A, Wittmann JC, Lotz B. Journal of Polymer Science, Part B: Polymer Physics 2002;40:2504–15.
[49] Marco C, Gomez MA, Ellis G, Arribas JM. Journal of Applied Polymer Science 2002;86:531–9.
[50] Alamo RG, Kim MH, Galante MJ, Isasi JR, Mandelkern L. Macromolecules 1999;32:4050–64.
[51] Lotz B, Graff S, Straupé C, Wittmann JC. Polymer 1991;32:2902–10.
[52] Foresta T, Piccarolo S, Goldbeck-Wood G. Polymer 2001;42:1167–76.
[53] Nakafuku C. Polymer 1981;22:1673–6.
[54] Brückner S, Meille SV, Petraccone V, Pirozzi B. Progress in Polymer Science 1991;16:361–404.
[55] Mark JE. New York: AIP Press; 1996. p. 409–15 [chapter 30].
[56] Kalay G, Zhong Z, Allan P, Bevis MJ. Polymer 1996;37:2077–85.
[57] Turner-Jones A, Aizlewood JM, Beckett DR. Makromolekulare Chemie 1964;75:134–54.
[58] Somani RH, Hsiao BS, Nogales A, Fruitwala H, Srinavas S, Tsou AH. Macromolecules 2001;34:5902–9.
[59] Turner-Jones A. Polymer 1971;12:487–508.
[60] Brucato V, Piccarolo S, La Carrubba V. Chemical Engineering Science 2002;57:4129–43.
[61] Corradini P, Petraccone V, De Rosa C, Guerra G. Macromolecules 1986;19:2699–703.
[62] Schrauwen BAG, van Breemen LCA, Spoelstra AB, Govaert LE, Peters GWM, Meijer HEH. Macromolecules 2004;37:8618–33.
[63] Fujiyama M, Wakino T. Journal of Applied Polymer Science 1991;43:57–81.
[64] Laihonen S, Gedde UW, Werner PE, Matrinez-Salazar J. Polymer 1997;38:361–9.
[65] Laihonen S, Gedde UW, Werner PE, Matrinez-Salazar J. Polymer 1997;38:371–7.
[66] Guinier A, Fournet G. Small-angle scattering of X-rays. New York: Wiley; 1955.
[67] Chen HB, Karger-Kocsis J, Wu JS, Varga J. Polymer 2002;43:6505–14.
[68] Pukánszky B, Mudra I, Staniek P. Polymer 1997;19:617–26.
[69] Odell JA, Grubb DT, Keller A. Polymer 1978;19:617–26.
[70] Bashir Z, Odell JA, Keller A. Journal of Materials Science 1984;19:3713–25.
[71] Bashir Z, Odell JA, Keller A. Journal of Materials Science 1986;21:3993–4002.
[72] Hobbs JK, Humphris ADL, Miles MJ. Macromolecules 2001;34:5508–19.